RSC Advances

ROYAL SOCIETY OF CHEMISTRY

www.rsc.org/advances

Cite this: DOI: 10.1039/c0xx00000x

www.rsc.org/xxxxxx

ARTICLE TYPE

Properties of cobalt nanofibers-based magnetorheological fluids

Xufeng Dong,*[a] Yu Tong,[a] Ning Ma,[b] Min Qi*[a] , and Jinping Ou[b,c]

Received (in XXX, XXX) Xth XXXXXXXXX 20XX, Accepted Xth XXXXXXXXX 20XX
DOI: 10.1039/b000000x

Co nanofibers were synthesized by a surfactant-assistant solvothermal method. They were characterized by XRD, EDS, SEM, TEM and SQUID. The results indicated that the obtained products were hexagonal close-packed cobalt nanofibers with high purity. They presented large length to diameter ratio, and a high saturation magnetization of 142 emu g^{-1}. Two magnetorheolgical (MR) fluids were prepared by the Co nanofibers and carbonyl iron particles with 12% particles volume fraction, respectively. Their magnetorheological properties and sedimentation stability was tested and compared. The results indicated that the Co nanofibers-based MR fluid presented higher yield stress than the carbonyl iron particles-based one at low field levels (0~150 kA/m). The strong chains or column structure caused by the specific morphology and high magnetization of the Co nanofibers is responsible for their significant MR properties. In 15 days setting, the Co nanofibers-based MR fluid presented little sedimentation, while the sedimentation ratio of the carbonyl iron particles-based MR fluid was 50%. The Co nanofibers are ideal candidates to prepare MR fluids with good sedimentation stability as well as good magnetorheological properties.

1 Introduction

Magnetorheological (MR) fluids are suspensions composed of magnetizable particles dispersed in a non-magnetizable carrier fluid. [1,2] Without a magnetic field, they are Newtonian fluids with free flow. When a magnetic field is applied, they become semi-solid materials, or Bingham fluids, with a yield stress.[3-6] The yield stress can be reversibly controlled by magnetic field strength, which makes MR fluids are successfully used in clutches, dampers and actuators in various fields. Typically, they are used in semi-active controllable fluid dampers for vehicles and buildings protection against vibrations.[7-13]

Carbonyl iron (CI) particles exhibit high magnetic permeability and high saturation magnetization. Therefore, they have been widely used as the magnetic phase to prepare MR fluids. The MR fluids fabricated with silicone oil and micro CI particles with high concentration show great yield stress (~100 kPa) at 250 kA/m. [14,15] However, still some problems exist, which prevent MR fluids from further applications. One problem is that the MR fluids with better MR properties than the CI particles-based fluids are in need. Another one is the CI particles-based MR fluids often subject to thickening after prolonged use.[16,17] Adding surfactant or coating polymer could improve the sedimentation stability to some extent, but at the cost of the MR effect.[18-20] Recent theoretical studies indicated that using rod-like or fiber-like particles could fabricate MR fluids that would have more significant MR effect and better sedimentation stability than those with sphere-like particles.[21,22] Unfortunately, it is difficult to prepare iron particles with rod or fiber morphology. In 2010, Juan de Vicente et al prepared iron particles with different morphologies by using a two-step synthesis route, and studied the effect of particle shape on MR properties of the MR fluids with low particles volume fraction.[23] However, the influence of the particle shape on sedimentation properties of MR fluids was seldom investigated. Besides, it is more meaningful to prepare MR fluids with comparable yield stress to commercial CI particles-based materials.

Compared with iron particles, the morphology of the cobalt particles can be easily controlled.[24-26] Considering cobalt is also a ferromagnetic material, cobalt particles with fiber-like morphology may be used to prepare a MR fluid with high particle content to verify the benefits of the fiber shape.[27] In this study, cobalt nanofibers, which also present high saturation magnetization, were synthesized by using a solvothermal method. A MR fluid based on the Co nanofibers was prepared with 12% particles volume fraction. Its magnetorheological properties and sedimentation stability were tested and compared with the MR fluid with commercial spherical CI particles.

2. Experimental

2.1 Preparation and characterization of cobalt nanofibers

Co nanofibers were synthesized by a surfactant-assistant solvothermal method. All chemicals were of analytical grade and used without further purification. In a typical procedure, firstly 1.1896 g of $CoCl_2$•$6H_2O$ and 70 μl of Brij30 were dissolved into

[a] *School of Materials Science and Engineering, Dalian University of Technology, Dalian 116024, China. Email:dongxf@dlut.edu.cn*
[b] *School of Civil Engineering, Dalian University of Technology, Dalian 116024, China.*
[c] *current address: School of Civil Engineering, Harbin Institute of Technology ,Harbin, 150090, China*

35 ml of ethylene glycol under magnetic stirring until a homogeneously red solution was formed. Then 0.5 g of PVP was added slowly to the above solution with simultaneous strongly agitation. Subsequently, 10 ml of ethylenediamine and 10 ml of NaOH solution (5 M) of deionized water were added dropwise to the above solution with simultaneous strongly agitation. After refluxing for 30 min, the resulting mixture was transferred into a 100 ml Teflon-lined autoclave, which was sealed tight and maintained at 180 °C for 24 h. After being cooled to room temperature naturally, the precipitates were obtained by centrifugation. The powder was thoroughly rinsed with distilled water and ethanol, followed by the removal of the residual solvent through drying at 50 °C for 24 h to obtain the final products.

The phases were identified by means of X-ray diffraction (XRD) with an Empyrean X-ray diffracometer with Cu Kα radiation (λ=1.5418 Å) at a scan rate of 0.04 s^{-1}. The distribution of the particle size was obtained by a laser diffraction particle size analyzer (Mastersizer 2000). The morphology and composition of the products were investigated by a JSM-5600LV scanning electron microscopy (SEM) with X-ray energy-dispersive spectroscopy (EDS). Transmission electron microscopy (TEM) observation was obtained on a Tecnai G220 S-Twin microscope. Magnetic measurements were carried out using a Quantum Design superconducting quantum interference device (SQUID) magnetometer (MPMS-XL-7) at fields up to 10 kOe.

2.2 Preparation and evaluation of Co nanofibers-based MR fluid

Carbonyl iron micro-particles purchased from Jiangyou Hebao Nanomaterial Co., Ltd. were used to produce the CI particles-based magnetorheological fluid. Silicon oil with a dynamic viscosity of 0.5 Pa·s was used as the carrier liquid. CI particles and Co nanofibers were mixed with silicone oil to prepare two different MR fluids, the particle volume fraction of which is 12%, respectively. They are named as CI-MRF and CoF-MRF in short in the following text.

Viscosity-shear rate curves at zero magnetic field, shear stress-shear rate curves at different magnetic fields, and dynamic shear moduli under different strain amplitude and angular frequency were measured by using a rheometer Physica MCR301 fitted with a magneto-rheological module, which can apply different magnetic fields by changing direct current. The diameter and the gap of the parallel-plate system were 20 mm and 1 mm, respectively. All the measurements were performed at room temperature. The sedimentation experiments were carried out at room temperature by using cuvettes. The sedimentation ratio, defined by the height percentage of the particle-rich phase relative to the total suspension height, was used to evaluate the sedimentation stability of the MR fluids.

3. Results and discussion

3.1 Properties of Co nanofibers

The size and morphology of the Co nanofibers were examined by SEM and TEM. A typical SEM image (Fig.1a) reveals that the products are Co nanofibers, whose length is in the range several tens micrometers to hundreds of micrometers. The TEM image of the Co nanofibers is shown in Fig.1b. It indicates the diameter of each nanofiber is uniform over its length. The average diameter is less than 100 nm. Figure 2 shows the particle size distribution of the Co nanofibers and the CI particles. It indicates the two kinds of particles have similar equivalent scattering diameter. For Co nanofibers, the equivalent scattering diameter is equivalent to their length. Since the average length of the Co nanofibers is ~20μm, their average length to diameter ratio is larger than 200.

The XRD pattern of the Co nanofiber is shown in Fig.3. All the diffraction peaks can be indexed as Co with hexagonal structure. The lattice constants of a=2.506 Å and c=4.072 Å are consistent with the standard card JCPDS card No. 05-0727 (space group $P6_3/mmc$). No obvious peaks resulted from impurities of cobalt oxides or hydroxides are observed, indicating that the nanostructures obtained by the synthetic route consist of a pure hcp phase. The average crystal size calculated based on the Scherrer Equation is 36 nm. The selected-area electron diffraction (SAED) pattern indicates the Co nanofibers are single-crystalline that grow along the (110) direction.[27] Figure 4 shows the EDS of the as-prepared products, which presents significant signals for Co. The small amount of carbon detected in Fig.4 is possibly from the remaining of some surfactant on the surface.

Figure 5 shows the magnetic hysteresis loops of the Co nanofibers and the CI particles at 300 K. The saturation magnetization (M_s) of the Co nanofibers is 142 emu g^{-1}, which is sight lower than their bulk counterpart (168 emu g^{-1}), but much lower than that of the CI particles (193 emu g^{-1}). The coercivity of the Co nanofibers is 343.2 Oe, which is much larger than that of bulk cobalt (10 Oe). It can be attributed to their small size, remarkable shape anisotroty, and hcp crystal structure. On contrast, the CI particles exhibit little coercivity. At low field levels, the magnetization intensities of two kinds of particles are nearly equal, while at high field levels, the CI particles presents larger magnetization intensity.

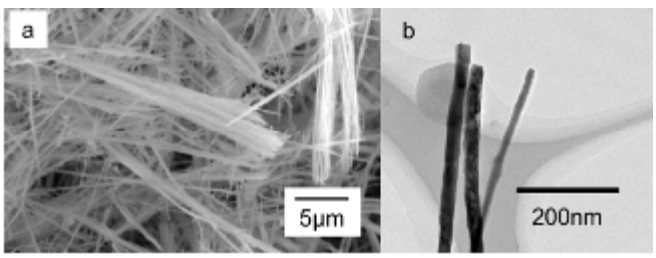

Figure 1. (a) SEM image and (b) TEM image of the Co nanofibers

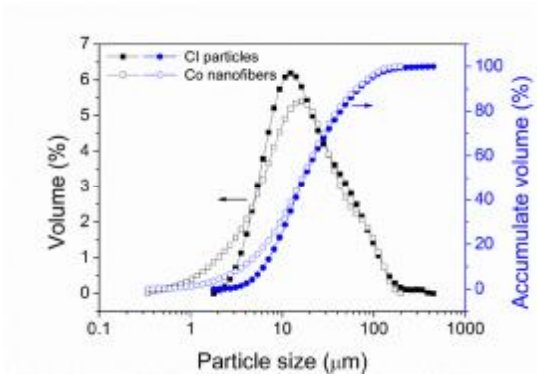

Figure 2. Particle size distribution of the Co nanofibers and the CI particles

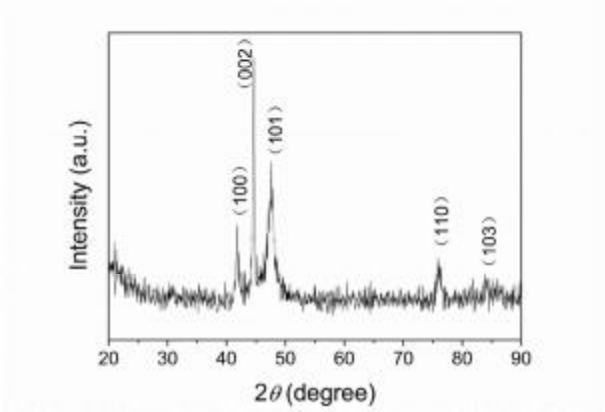

Figure 3. XRD pattern of the Co nanofibers

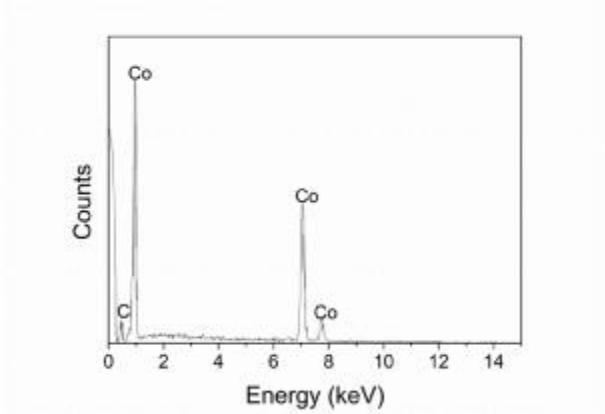

Figure 4. EDS pattern of the as-prepared Co nanofibers

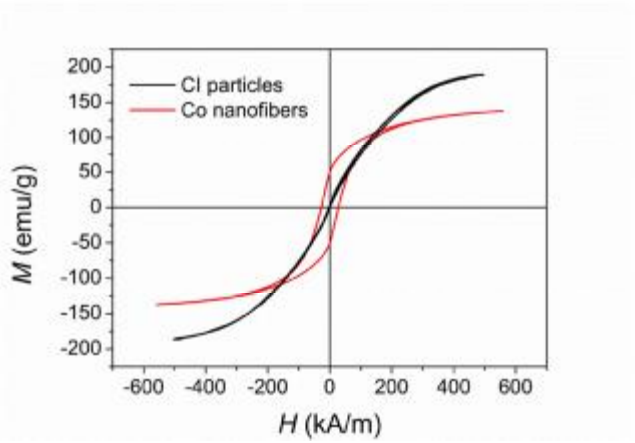

Figure 5. Magnetic hysteresis loop of the Co nanofibers and the CI particles at 300 K

3.2 Properties of MR fluids based on Co nanofibers

Figure 6 presents the flow curves at zero field for the two MR fluids containing 12% CI particles and Co nanofibers by volume fraction, respectively. Due to the shear-thinning effect, the viscosities of the two fluids decrease dramatically with increasing shear rate at low shear rate levels, and then the changes become gently and reach a constant value at high shear rate levels. At low shear rate, CoF-MRF presents lower viscosity than CI-MRF. The possible reason is that the length direction of the Co nanofibers orients to the flow direction under shear load. However, at high shear rate there are little differences on viscosity between the two fluids. It indicates the influence of the particle morphology on the viscosity of the MR fluids can be ignored at high shear rate levels. The possible reason is that the particles aggregation completely decomposes at high shear rate without respect to the particle morphology, in which case the particle volume fraction plays the dominate role on the viscosity of the MR fluids.

Figure 7 represents shear stress as a function of shear rate for CI-MRF and CoF-MRF under different magnetic field strengths (0kA/m, 82 kA/m, 142 kA/m, 186 kA/m, 220kA/m and 250kA/m). The two MR fluids present Newtonian behavior in absence of magnetic field, the relationship between shear stress and shear rate is a straight line passed the original point. At a magnetic field, typical Bingham behavior can be observed for both of the two MR fluids. The fitting curves based on the Bingham model agree well with the experimental data. The vertical intercept of each fitting curve can be considered as the yield stress under the corresponding magnetic field. Therefore, the dependence of the yield stress of the two MR fluids on magnetic field is obtained, as shown in Fig.8. Their yield stress increases with increasing magnetic field strength, indicating significant MR effect. The formation of robust columns composed by magnetic particles is responsible for the MR effect. At 250 kA/m, the yield stresses of CI-MRF and CoF-MRF are 60 kPa and 41 kPa, respectively. Although the yield stress of CoF-MRF is lower than that of CI-MRF at high magnetic field levels, it is higher than the later at low field levels (0~150 kA/m). The main reason is that at low magnetic field, the fiber morphology of the magnetic phase plays a dominate role for the high yield stress of CoF-MRF. The dipole-dipole interaction among the adjacent nanofiers is stronger than that among the sphere-like particles, which have been stated in several theoretical studies. Another reason that cannot be neglected is that the Co nanofibers present comparable magnetization intensity with CI particles at low field levels, as shown in Fig.5. Besides, the demagnetization effect of sphere-like particles is much more significant than that of the fiber-like particles, which further makes the magnetization intensity of the Co nanofibers is higher than that of the CI particles. As stated in previous studies, the yield stress of MR fluids positively depends on the magnetization intensity of the dispersing particles.[3,23] This also can explain that the CI-MRF exhibits higher yield stress than the CoF-MRF. The excellent MR effect of CoF-MRF at low magnetic field is meaningful, because in most applications it is difficult to get a high magnetic field strength. Besides, the yield stress that exceeds 30 kPa can meet the requirement in most fields.

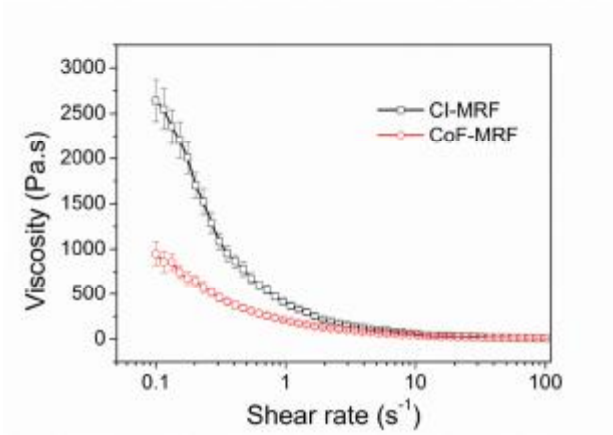

Figure 6 Dependence of viscosity of CI-MRF and CoF-MRF on shear rate

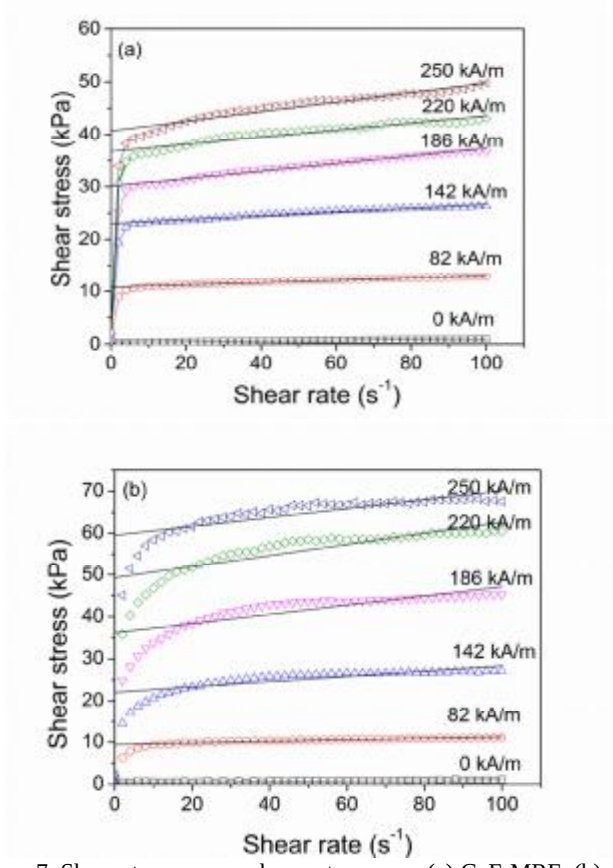

Figure 7. Shear stress versus shear rate curves: (a) CoF-MRF, (b) CI-MRF

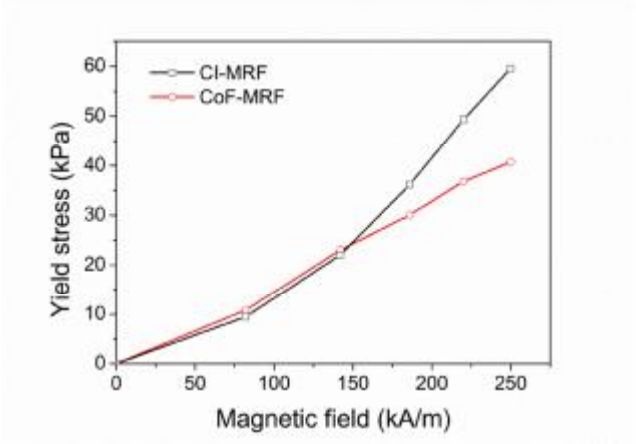

Figure 8. Dependence of yield stress of CI-MRF and CoF-MRF on magnetic field

Figure 9 shows the dependence of the dynamic shear moduli of CoF-MRF and CI-MRF, including storage modulus *G'* and loss modulus *G"*, on strain amplitude at a constant angular frequency of 10 rad/s. Without a magnetic field, their storage modulus and loss modulus decrease with increasing strain amplitude, and the storage modulus is smaller than the loss modulus when the strain amplitude reaches a small value (0.1% for CoF-MRF, and 0.2% for CI-MRF), indicating a liquid-like state in absence of the magnetic field. When a magnetic field is applied, their storage modulus keeps unchanged at low strain amplitude and then decreases with increasing strain when it reaches a critical value, while the loss modulus initially slightly increases and then decreases. Below the critical strain amplitude, the MR fluids are considered in linear viscoelastic (LVE) region. When the strain amplitude exceeds the critical value, the chains or columns formed by the magnetized particles becomes unstable, and the MR fluids are in nonlinear viscoelastic region. As the magnetic field strength rises, the critical strain amplitude that the storage modulus begins to decline increases, which is highlighted by the red arrows in the two subfigures. It indicates that the chain structure becomes more rigid at higher magnetic field levels. Besides, it can be seen from Figure 9 that at low strain amplitude levels, the storage modulus is higher than the loss modulus, indicating a solid-like state due to the formation of chains or columns along the field direction. However, at high strain amplitude levels, the storage modulus is lower than the loss modulus, indicating the failure of the chain structure due to the complete separation of the particles. At the same magnetic field, the cross point between the storage modulus curve and the loss modulus curve corresponds to the strain amplitude that the MR fluids are transforming from solid-like state to liquid state. It can be expected that the cross point move to high strain amplitude with increasing magnetic field, even some of the points are not shown in the two subfigures due to the limit range of the strain amplitude in the tests. It also indicates the chains or columns composed by the particles are more rigid under higher magnetic field.

Figure 10 further shows the dependence of the critical strain amplitude that keeps the MR fluids in LVE region on magnetic field. As the magnetic field increases, the critical strain amplitude promotes. At the same magnetic field, the Co

nanofibers-based MR fluid presents higher critical strain amplitude than the CI particles-based MR fluid. It further confirms the chains or columns formed by the Co nanofibers are stronger than the CI particles. The unique morphology of the Co nanofibers may be responsible for their robust structure. Interestingly, even at high magnetic field levels, the CoF-MRF still exhibits higher critical strain amplitude. However, at high field levels, the CI-MRF has higher yield stress, as shown in Fig.8. It indicates there may be some other factors that influence the yield stress of the MR fluids, which should be further studied in future.

Small-amplitude oscillatory shear frequency sweep curves at a constant strain (0.01%) and different magnetic field strength (0kA/m, 82 kA/m, 142 kA/m, 186 kA/m, 220kA/m and 250kA/m) are presented in Fig.11 for the two MR fluids. As it is shown, under a magnetic field, their storage modulus initially increases with increasing angular frequency. Nevertheless, it remains nearly unchanged when the angular frequency exceeds a critical value. The possible mechanism is that the chain or column structure formed by the magnetized particles becomes unstable under low loading frequency. As the magnetic field increases, the chain or column structure becomes more rigid; as a result, the critical angular frequency decreases. It is also can be observed in Fig.11 is that under the same magnetic field, the CoF-MRF presents higher storage modulus compared with the CI-MRF.

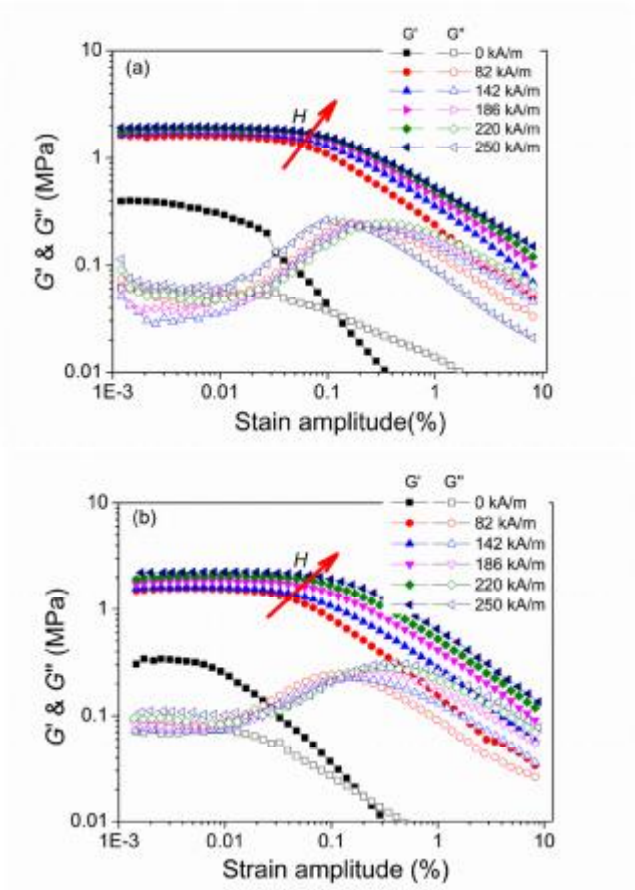

Figure 9 Dependence of the dynamic shear moduli (storage modulus *G'* and loss modulus *G"*) of (a) CoF-MRF and (b) CI-MRF on strain amplitude at a constant angular frequency of 10 rad/s

Since both of the two MRFs are in the LVE region at 0.01% strain amplitude without respect to the applying magnetic field, the data at 0.01% in Fig.9 are extracted to compare their dynamic moduli, as shown in Fig.12. The storage modulus of the two MRFs increases with increasing magnetic field, indicating more rigid chains or columns are formed by the particles. Besides, under low field levels (0~150kA/m), the CoF-MRF present higher storage modulus than the CI-MRF, which is due to the fiber-like morphology, high magnetization, and low demagnetization factor of the Co nanofibers. Owing to the similar trend of yield stress and storage modulus with respect to magnetic field and particle morphologies, the increase in yield stress can be partially attributed to the increase in *G*'. Nevertheless, it appears unlikely for them to grow simultaneously, indicating the possible existence of some other reasons for the increase in yield stress observed.

Figure 13 shows the dependence of sedimentation ratio on time for the two MR fluids. In the first 2 days, CI particles settled down rapidly, and the sedimentation ratio of CI-MRF was ~50%. Then the sedimentation velocity becomes slow, and the sedimentation ratio tended to a stable value. In contrast, the sedimentation ratio of CoF-MRF kept at ~100% in the recording 15 days, indicating little Co nanofibers settled. The CoF-MRF presents much more excellent sedimentation stability compared with the common CI-MRF. The one-dimensional nanoscale of the Co nanofibers is the main reason for its good sedimentation stability. On one hand, the Brownian motion for the nanofibers in the fluid is intense enough to balance the gravity. On the other hand, the Co nanofibers may form stable network due to their large length to diameter ratio, which is also beneficial for the improvement of the sedimentation stability.

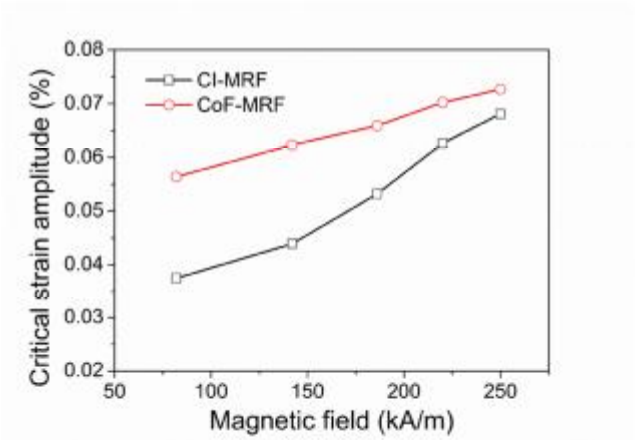

Figure 10 Dependence of the critical strain amplitude that keeps the MR fluids in LVE region on magnetic field.

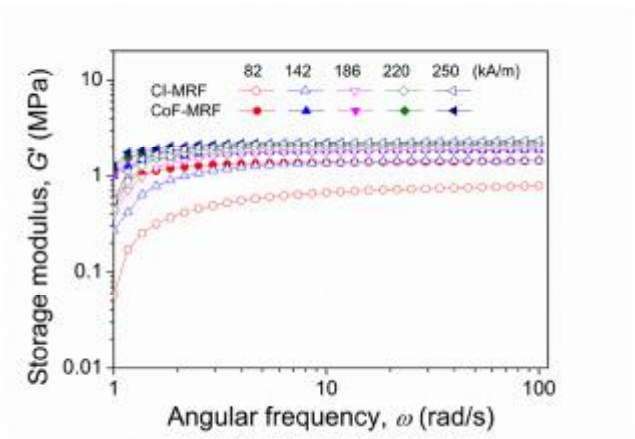

Figure 11 Dependence of the storage modulus of CoF-MRF and CI-MRF on angular frequency at a constant stain amplitude of 0.01%

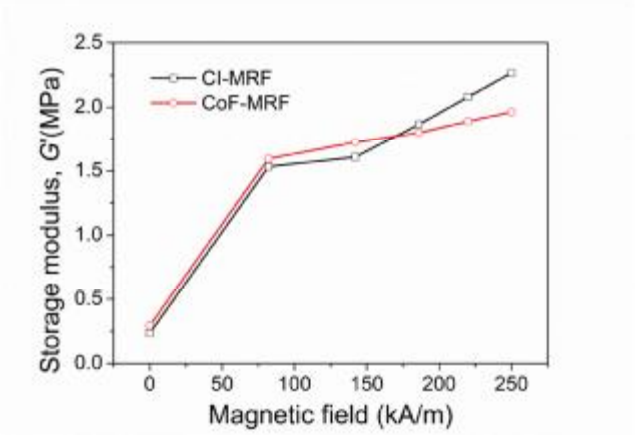

Figure 12 Dependence of the storage modulus of CoF-MRF and CI-MRF on mangetic fieldd at a constant stain amplitude of 0.005% and a constant angular frequency of 10 rad/s

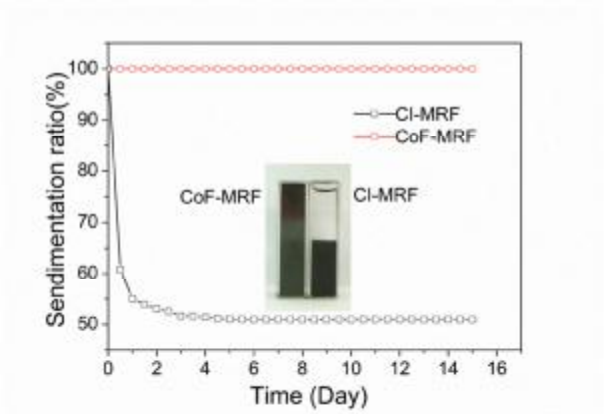

Figure 13. Sedimentation curves of CoF-MRF and CI-MRF. The inserted picture is the photograph of the two MR fluids after 15 days 'setting without disturb

4 Conclusions

Co nanofibers were synthesized and used to prepare a magnetorheological fluid with 12% additive volume fraction. The Co nanofibers present high saturation magnetization and large length to diameter ratio. At low field levels, the Co nanofibers-based MR fluid exhibits larger yield stress compared with the common carbonyl iron particles-based MR fluid with the same particle volume fraction. More strong chain structure may be formed in the Co nanofibers-based MR fluid due to the fiber-like morphology of the particles, which gives rise to their high storage modulus in the linear viscoelastic region. The most remarkable advantage of the Co nanofibers-based MR fluid is its excellent sedimentation stability; no obvious settling was observed during 15 days standing.

Acknowledgements

This research is financial funded by the National Natural Science Foundation of China under the grant number of 51478088 and 51108062.

Notes and references

1 J. Rabinow, *AIEE Trans.*, 1948, 67, 1308.
2 J. Vicente, D. J. Klingenberg and R. Hidalgo-Alvarez, *Soft Matter*, 2011, 7, 3701.
3 J. M. Ginder and L. C. Davis, *Appl. Phys. Lett.*, 1994, 65, 3410.
4 J. D. Carlson and M. R. Jolly, *Mechatronics*, 2000, 10, 555.
5 J. P. Segovia-Gutiérrez, J. de Vicente, R. Hidalgo-Álvarez and A. M. Puertas, *Soft Matter*, 2013, 9, 6970.
6 H. Chiriac and G. Stoian, *Journal of Physics: Conference Series*, 2010, 200, 072095.
7 S. J. Dyke, B. F. Jr Spencer and J. D. Carlson, *Smart Mater. Struct.*, 1996, 5, 565.
8 X. C. Guan, J. H. Li and J. P. Ou, *Engineering Mechanics*, 2005, 22, 207.
9 Y. Xu, X. Gong, S. Xuan, W. Zhang and Y. Fan, *Soft Matter*, 2011, 7, 5246.
10 Y. Xu, X. Gong, T. Liu and S. Xuan, *Soft Matter*, 2013, 9, 7701.
11 Y. S. Jia and K. K. Zhou, *Journal of Mechanical Engineering*, 2009, 45, 246.
12 M. A. Liu, *Forest Engineering*, 2009, 25, 32.
13 Q. H. Nguyen and S. B. Choi, *Smart. Mater. Struct.*, 2009, 18, 1.
14 K. I. Jang, B. K. Min and J. Seok, *J. Magn. Magn. Mater.*, 2011, 323 1324.
15 J. Jiang, Y. Tian, D. Ren and Y. Meng, *Smart. Mater. Struct.*, 2011, 20, 085012.
16 Y. H. Kim, B. J. Park, H. J. Choi and Y. Seo, *Phys. Stat. Sol.*, 2007, 12, 4178.
17 M. T. López-López, A. Zugaldía, F. González-Caballero and J. D. G. Durána, *J. Rheol.*, 2006, 50, 543.
18 S. T. Lim, M. S. Cho, I. B. Jang and H. J. Choi, *J. Magn. Magn. Mater.*, 2004, 282, 170.
19 M. Sedlacik, V. Pavlinek, P. Saha, P. Svrcinova, P. Filip and J. Stejskal, *Smart. Mater. Struct.* , 2010, 19, 115008.
20 D. H. Wang and W. H. Lian, *Smart. Mater. Struct.*, 2011, 20, 023001.
21 R. C. Bell, E. D. Miller, J. O. Karli, A. N. Vavreck and D. T. Zimmerman, *International Journal of Modern Physics B*, 2007, 21, 5018.
22 M. T. López-López, G. Vertelov, G. Bossis, P. Kuzhira and J. D. G. Duránc, *J. Mater. Chem.*, 2007, 17, 3839.
23 J. de Vicente, F. Vereda, J. P. Segovia-Gutiérrez, M. del Puerto and R. J. Hidalgo-Álvarez, *J. Rheol.*, 2010, 54, 1337.
24 M. S. Wong, J. N. Cha, K. S. Choi, T. J. Deming and G. D. Stucky, *Nano Lett.*, 2002, 2, 583.
25 Y. Soumare, C. Garcia, T. Maurer, G. Chaboussant, F. Ott, F. Fiévet, J. Piquemal and G. Viau, *Adv. Funct. Mater.*, 2009, 19, 1971.
26 Y. Zhang, S. W. Or and Z. Zhang, *RSC Advances*, 2011, 1, 1287.
27 X. Dong, M. Qi, Y. Tong and F. Ye, *Materials Letters*, 2014, 128, 39.